SciMedCentral
Bringing Excellence in Open Access

Journal of Embryology & Developmental Biology

Original Research Article

Effects of Substrate Stiffness on Cardiac-fated Cells

Julia A. Henkels*, Todd Sulchek, Andrés J. García, Evan A. Zamir

George W. Woodruff School of Mechanical Engineering, Georgia, USA

***Corresponding author**
Julia A. Henkels, Parker H. Petit Institute for Bioengineering and Bioscience
Georgia Institute of Technology
Atlanta, Georgia 30332, USA
Tel: +1-646-543-3635
Email: jhenkels3@gatech.edu

Submitted: 04 June 2017

Accepted: 02 October 2017

Published: 18 December 2017

Keywords

- Development
- Cardiogenesis
- Vinculin
- Sarcomeric myosin heavy chain
- E-cadherin
- Primitive streak
- Smooth muscle alpha-actin

Abstract

As cardiac-fated cells traverse the course of differentiation into cardiac myocytes, the sequence, magnitude, and spatiotemporal map of biomechanical signals that may influence cardiogenesis have not been fully explored. Whereas several studies have examined the induction of cardiogenesis on different extracellular matrix proteins and substrates, none have examined the effects of substrate stiffness prior to the onset of cardiac differentiation in cardiac-fated cells. We investigate the effects of substrate stiffness on precardiac cell behaviors in an in vitro setting. The cells in the anterior portion of the primitive streak are fated to form the heart, and we show differing levels of smooth muscle α-actin expression (and E-cadherin) on substrates of differing moduli, which suggests that substrate stiffness may play a role in cardiac differentiation. However, we could not detect changes in the presence of sarcomeric myosin heavy chain expression or the occurrence of beating cultures, which suggests that although cardiac-fated cells show a sensitivity to substrate stiffness, different or more sensitive tests would be required to confirm a functional difference at this early stage.

Abbreviations: PS: primitive streak; **HFRs**: heart-forming regions; **HH**: Hamburger Hamilton; **SMA**: Smooth muscle α-actin; **PDMS**: polydimethylsiloxane; **ECad**: E-cadherin; **VIN**: vinculin; **FN**: fibronectin

INTRODUCTION

Cells generate biochemical activity from mechanical stimuli (such as extracellular stiffness) in a process termed mechanotransduction, which is largely mediated at focal adhesion sites [1]. A mechanotransductive response to changes in substrate stiffness has been shown to regulate cell life and death [2,3], growth [2,3], shape [2,3,4,5], proliferation [6,7], adhesion [2,5,7,8,9], migration [5,10,11,12], contractility [2,10], differentiation [2,13,14], and disease pathologies, notably cancer metastasis [15,16]. Mechanosensing plays an important role in embryogenesis and tissue differentiation [17]. Here, we examine the role of substrate stiffness in cardiac-fated cells that will form the heart. In the area of regenerative medicine, an understanding of the effect of substrate stiffness on precardiac cells in the embryo is critical for the ongoing work of human induced pluripotent stem cell (hiPSC) differentiation into the cardiac lineage [18] and cardiac cell-therapy applications [19]. It has been shown that embryonic cardiomyocytes respond to changes in substrate stiffness [7,20,21] (Hamburger Hamilton [22] stages 18+) and that there are significant changes to the mechanical environment of the embryonic heart over time [23,24], but no studies have been completed to examine the role of substrate stiffness prior to heart formation and prior to the onset of cardiac differentiation in cardiac-fated cells.

In the avian pre-primitive streak blastula (Eyal-Giladi Kochav [EK] [25] stages X-XIV; stage EK XIV corresponds to Hamburger Hamilton stage 1), prospective heart cells occupy the posterior medial portion of the epiblast in a region termed Koller's sickle, from which the primitive streak (PS) extends [26]. These cells move anteriorly during PS formation during early stages of gastrulation, and at Hamburger Hamilton stage 3 (HH3), presumptive heart cells reside in the anterior half of the PS. By mid-primitive-streak stages (HH4), cardiogenic cell ingression is complete. After ingression, cardiac regions migrate anterolaterally (HH5 and HH6) to form a lateral plate mesoderm on each side of the PS, termed the precardiac mesoderm [27,28,29]. The most lateral portion of the lateral mesoderm are termed the heart forming regions (HFRs) [30]. These HFRs have been explanted and found to differentiate into heart muscle [31]. At HH6 cardiac precursors epithelialize, and during stage 7 they form the splanchnic (ventral) and somatic (dorsal) mesoderm separated by a space called the pericardial coelom

[32]. The coelom cavities migrate and join at the ventral midline of the embryo and continue to fuse in the anterior and posterior directions [33] at the 4-somite stage (HH8) in the quail embryo [34] and at the 7-somite stage (HH9) in the chick embryo [35] to form the primitive heart tube. Following these events, the heart tube loops and undergoes septation and valve formation.

Many markers have been shown to identify cardiac differentiation including N-cadherin [32] and myofibrillar proteins including troponin [36], cardiac C-protein [36], myosin heavy-chain [36,37,38], myosin light-chain, tropomyosin, actin isoforms [39], muscle α–actinin [40], and cNkx-2.5 [28]. Smooth muscle α-actin (SMA) expression first marks the onset of cardiac cell differentiation [41], and it is the major actin isoform in vascular tissue [39,30]. The HFRs begin to express the first cardiac-specific gene, SMA, at stage HH5. SMA mRNA was first discovered during the early stages of heart tube formation in stages HH8 and HH9 avian cardiac tissue [41]. The earliest detection of SMA transcripts in the embryo is stage HH5 in right and left anterior regions and is present in the coelom [30]. Translated SMA was first seen at stage HH9, detected exclusively in the heart [39]. It is first translated at HH7+, at the fusion of the bilateral heart forming regions [30]. Sarcomeric myosin heavy chain, a later-stage heart marker, is expressed at stage HH7+ in the chick embryo [37]. Atrial-specific myosin heavy chain (AMHC1) is transcribed at HH9 [38]. At HH12, the smooth muscle α-actin is down-regulated in the heart, remaining only in the conus, which forms the vascular trunks [41] and SMA is replaced by sarcomeric actin [39].

There have been many developmental cardiac differentiation studies using embryonic explants from gastrula and pre- gastrula avian embryos (stage HH1-3; 0-12 h of incubation) over the past twenty years, but most of these have been conducted on glass [29,40,42,43,44,45,46,47] or a collagen gel [48] or a floating filter raft [28]. It was recently shown that there is an optimal substrate stiffness for the contraction of differentiated embryonic cardiomyocytes harvested from embryonic avian hearts [20], and cardiac cells from formed embryonic hearts continue to show increased heart markers on increased substrate stiffnesses [21]. However, no rigorous study has been completed to examine the role of mechanics - specifically, substrate stiffness - in early heart development reminiscent of the body of previous work on gastrula and pre-gastrula embryos (0-12 h incubation, prior to heart formation). We recently characterized the stiffness of the pre- and post-primitive streak embryo, where precardiac cells reside and found that embryos at HH1 have an average stiffness of about 200 Pa [49]. Previous differentiation studies have not been carried out at this physiologic stiffness. The objective of this study was to determine the effects of substrate stiffness on cardiac induction. HH3 marks the final embryo stage prior to the onset of cardiac gene expression; the HH3 PS therefore provides a valuable source of undifferentiated cardiac-fated cells with which to study the relationship between substrate stiffness and cardiac induction. Cells were taken from 3-day-old quail hearts as a positive control for SMA-expressing cardiac cells.

MATERIALS AND METHODS

PDMS fabrication

Dow Corning Sylgard® 527 A/B Silicone (polydimethylsiloxane) Dielectric Gel was combined in ratios of 0.1:1 and 1.5:1 (A:B) (wt%) and mixed vigorously with a pipette tip for 5 min. 50 µL of the mixture was pipetted onto 18-mm glass coverslips in a Laurell Spin Coater (WS-400BZ-6NPP) and spun at 1500 rpm for 10 seconds. 0.1:1 coverslips were cured in a silanized dish at 90 °C for 24 h and 25 °C for 24 h. 1.5:1 coverslips were cured at 70 °C for 72 h and 25 °C for 24 h.

Atomic force microscopy

An MFP-3D atomic force microscope from Asylum Research (Santa Barbara, CA) (setup described previously [49]) was used to characterize the stiffness of the Sylgard® 527 substrates in ratios of 0.1:1 and 1.5:1 (A:B). To minimize in-plane stress and to simplify contact mechanics, a 15-µm-diameter polystyrene bead was attached to a Bruker triangular AFM cantilever. Samples were indented 5 times in different regions. Indentation force curves (force vs. indentation) were fitted to the Hertz model to determine the modulus for 0.1:1 PDMS indentations [49]. However, we found that the modulus varied with indentation depth for the "soft" 1.5:1 PDMS substrates. Therefore, using the Hertz model, we plotted the modulus vs. indentation depth for each indentation in 1.5:1 PDMS and averaged the moduli in the linear region of the curve [50]. Measurements were taken under water at room temperature in a 50-mm fluorodish from World Precision Instruments (Sarasota, FL). Three regions per sample were indented with 5 indentations per region across several sample preparations.

Fibronectin substrate coating

PDMS-coated coverslips were coated with fibronectin (FN) by incubating in 10 µg/mL FN (Gibco® Human Plasma Fibronectin, InvitrogenTM 33016-015) overnight at 37 °C and washed 3 times with sterile DPBS (+/+) (cellgro® 21-030-CV, henceforth called DPBS).

Anterior and posterior primitive streak culture

Embryos were cultured at stage HH3 (12-14 h) using the New egg culture technique [51]. Anterior and posterior PS explants (Figure 1) were cut using sterile glass needles pulled with a micropipette puller (Narishige Model PC-10) under a dissecting microscope (Leica MZ16F). Explants were placed on FN-coated PDMS substrates in serum-free media (RPMI 1640 + 1% ITS + 1% P/S) and were incubated at 37 °C for 72 h.

Cardiac cell isolation

Hearts were harvested from 3-day-old quail embryos with sterile glass needles (Narishige Model PC-10 micropipette puller). After incubating in 1x (0.05%) trypsin + 0.5 mM EDTA at 37 °C for 15 min and quenching with media (DMEM-F12 + 10% FBS + 1% P/S), the tissue was gently dissociated by 50 passes in a 2-mL pipette tube. Cells were pelleted at 500 rpm for 5 min, resuspended in fresh media, and seeded at a density of 6 hearts

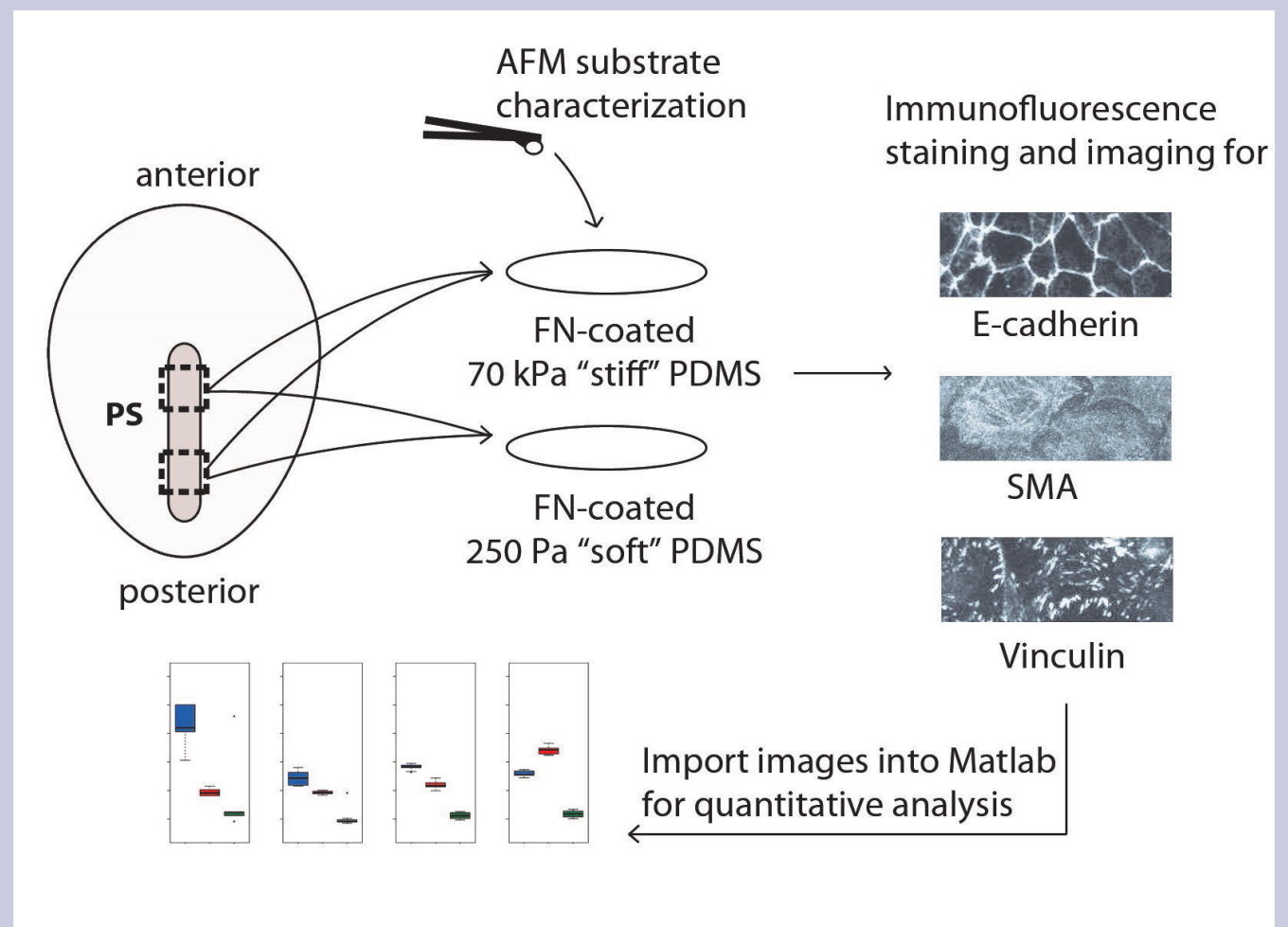

Figure 1: Explants from the anterior and posterior primitive streak were cultured on fibronectin-coated 70 kPa and 250 Pa Sylgard 527 PDMS. Samples were stained with ECad, SMA, and VIN; the same field was imaged for all 3 stains. Images were exported to Matlab for quantitative analysis.

per 18-mm substrate in a 12-well plate and incubated at 37 °C for 72 h.

Immunofluorescence staining and imaging

PS and cardiac cell cultures were rinsed with ice-cold DPBS, incubated in ice-cold Cytoskeleton (CSK) Buffer (10 mM PIPES buffer, 50 mM NaCl, 150 mM sucrose, 3 mM MgCl2, 1 mM PMSF, 1 μg/mL leupeptin, 1 μg/mL aprotinin, 1 μg/mL pepstatin) for 2 min, incubated in 2 separate washes of CSK buffer with 0.5% (v/v) Triton X-100, and fixed for 30 min in 3% paraformaldehyde in DPBS at 25 °C [52]. Samples were washed 3 times with DPBS and blocked with blocking buffer (3% bovine serum albumin in DPBS + 0.05% sodium azide) for 1 h at 25°C. Samples were then incubated with a primary vinculin antibody (SIGMA V4505, clone VIN-11-5) at a concentration of 2.6 mg/mL diluted in blocking buffer for 1 h at 25 °C, rinsed 3 times with DPBS for 5 min each, incubated with Alexa Fluor® 488-conjugated goat anti-mouse isotype-IgG1-specific secondary (Jackson ImmunoResearch 115-545-205) at 14 μg/mL, and rinsed 3 times with DPBS for 5 min each. Smooth muscle α-actin (SMA) monoclonal antibody (Pierce MA1-06110, isotype IgG2a, clone 1A4) was directly conjugated to rhodamine phalloidin using an EasyLink Rhodamine Conjugation Kit (Abcam ab102915). Samples were incubated with the SMA direct conjugate (1 μg/mL) and Alexa Fluor® 647 mouse anti-E-Cadherin direct conjugate (BD Pharmingen 560062, isotype IgG2a) at 5 μg/mL for 1 h at 25 °C, then rinsed 2 times with DPBS and once with Millipore water for 5 min each. Samples from each experimental group were labeled with isotype controls at the same concentration as the corresponding primary antibody for 1 h at 25 °C (Alexa Fluor® 647 mouse IgG2a Isotype Control, BioLegend 400234; Dylight™ 488 conjugate IgG1 Isotype Control, Enzo Life Sciences ADI-SAB-600-488; Rhodamine-conjugated mouse IgG2a Isotype Control, Rockland 010-0041), then rinsed 2 times with DPBS and once with Ultrapure Milli-Q® water (TOC<10ppb, 18.2MΩ·cm at 25 °C) for 5 min each.

Sarcomeric myosin fixation and staining was as follows. Samples were washed 3 times with DPBS and fixed for 1 h at 4 °C in fixation medium (by volume, 60% EtOH, 3.2% formaldehyde, and 4.3% acetic acid in DIH20) [53]. After 3 more washes with DPBS, samples were blocked with blocking buffer (5% goat serum in DPBS) for 1 h at 25 °C. After 3 DPBS washes, samples were stained with MF20 primary antibody (Developmental Hybridoma, 1:500 in blocking buffer) for 1 h at 37 °C, washed 3 times with DPBS, and blocked with blocking buffer for 10 min at 25 °C. After 3 DPBS washes, samples were incubated with Dylight 649 secondary (donkey anti-mouse, Jackson ImmunoResearch,

1:200 in blocking buffer) for 1 h at 37 °C. Following 3 washes with DPBS and 10 min of blocking at 25 °C, samples were incubated with 1 μM SYTOX® Green Nucleic Acid Stain (Molecular Probes®, Invitrogen™ S7020) in blocking buffer for 1 h at 25 °C, then rinsed 2 times with DPBS and once with Ultrapure Milli-Q® water for 5 min.

Samples were mounted with ProLong® Gold Antifade Reagent. Images were taken on a Leica DMI6000B inverted microscope with a Ludl Mac5000 controller and Hamamatsu ORCA-ER camera at 10x with 1x1 binning. Exposure time was set using isotype controls before imaging each experimental group.

Imaging processing and statistical analysis

Images were corrected for background by using a sample in every experimental group stained with an isotype control antibody to set the exposure time such that unspecific binding was not detected. Images were imported into Matlab, and the absolute value of the intensity per image was calculated using a sum command of all pixels. Then the fluorescence intensities for each stain across all samples was plotted (Figure 2M-P).

To allow for comparisons between the intensities of the stains in different regions and to address the heterogeneity of the samples, we developed an unbiased method to quantify differences between regions. We noticed that across all repetitions of these experiments, the intensity of vinculin staining appeared to be at a similar level for all sample groups and provided a "baseline" stain across all groups regardless of region or substrate. In an effort to take into account field-to-field differences between the 10x images (i.e., cell spreading, sample morphology, and cell count), we normalized the E-cadherin and SMA intensities to the vinculin fluorescence intensity (E/V and S/V) for each sample (Figure 2Q-T) to express the E-cadherin and SMA staining levels while accounting for differences between fields. To calculate the ratios of SMA or E-cadherin intensity to vinculin intensity for the same 10x field, the summed intensity value of the SMA or E-cadherin image was divided by the vinculin intensity sum. This method normalized the protein expression differences and provided the clearest method for the purpose of comparison.

It is important to note that the representative images shown in this study have been optimized to display cell features of interest; however, all quantification has been conducted on raw images using tif files taken directly from the microscope.

Statistical analyses were performed in R (http://www.r-project.org), a free software environment for statistical computing and graphics. The absolute intensity values per field per stain and intensity ratio values per field were imported into R. First, an omnibus ANOVA test was used to detect differences between all sample groups and test for interaction effects. There were interaction effects between the independent variables of different surfaces (glass, 70 kPa PDMS, 250 Pa PDMS) and cell type (anterior PS epithelial and mesenchymal cells, posterior mesenchymal cells, and cardiac cells), which means these two variables were separated for analysis. Pairwise t-tests were used to determine differences between absolute intensity values and intensity ratio values (S/V and E/V) for each sample group.

For MF20-stained cells, images of each sample (nuclei stain and MF20 stain) were imported into Matlab. Images were thresholded to count nuclei and determine overall cell count, and nuclei/MF20 overlapped regions were counted to determine MF20-positive cell count. Percentages of MF20-positive cells per sample were imported into R. An initial omnibus ANOVA test yielded significant differences between groups and no interaction effects. Pairwise comparisons were carried out using the pairwise t-test.

A chi-squared contingency table was used to determine whether there were differences in the frequency of beating cultures on "soft" and "stiff" PDMS.

RESULTS

Substrate mechanical characterization

The substrate used in this study, polydimethylsiloxane (PDMS) (Dow Corning Sylgard® 527 A/B Silicone Dielectric Gel) was chosen for its range of moduli in addition to its biological inertness and optical transparency. Coverslips were spin-coated and cured, then tested on an atomic force microscope.

The Hertz Model, a linear contact mechanics model, was used to determine a modulus from the force vs. indentation curves. Deviations from the Hertz Model indicate nonlinearity. Indentations were fit to the Hertz model for 0.1:1(A:B) "stiff" PDMS indentations; however, we found that for the 1.5:1(A:B) PDMS "soft" substrates, the Hertz model often did not fit the entire length of the force curve and would align with only a region of the curve. Therefore, using the Hertz model, we plotted the modulus vs. indentation depth for each indentation in 1.5:1 PDMS and averaged the moduli in the linear region of the curve. We show the measured moduli per region of each PDMS ratio in Table 1. The variation in modulus across the regions shows the heterogeneity of the sample. The average moduli of 250 ± 190 Pa (for 1.5:1 PDMS) and 70 ± 9 kPa (for the 0.1:1 PDMS) will be referred to throughout the remainder of this paper as "soft" and "stiff", respectively, for simplicity.

Table 1: AFM characterization of PDMS substrates

0.1:1 (A:B) PDMS		1.5:1 (A:B) PDMS	
Region	**Modulus (kPa) ± S.D.**	**Region**	**Modulus (Pa) ± S.D.**
1	66.2 ± 15.1	1	191.4 ± 75.0
2	79.8 ± 0.9	2	199.6 ± 143.6
3	49.3 ± 5.6	3	315.8 ± 261.6
4	65.1 ± 15.3	4	289.7 ± 253.9
5	69.2 ± 9.7	5	283.8 ± 149.0
6	85.4 ± 9.3	6	259.4 ± 279.4
7	74.5 ± 11.0		
8	71.1 ± 8.5		

Abbreviations: polydimethylsiloxane (PDMS), standard deviation (S.D.), ratio of polydimethylsiloxane components (A:B)

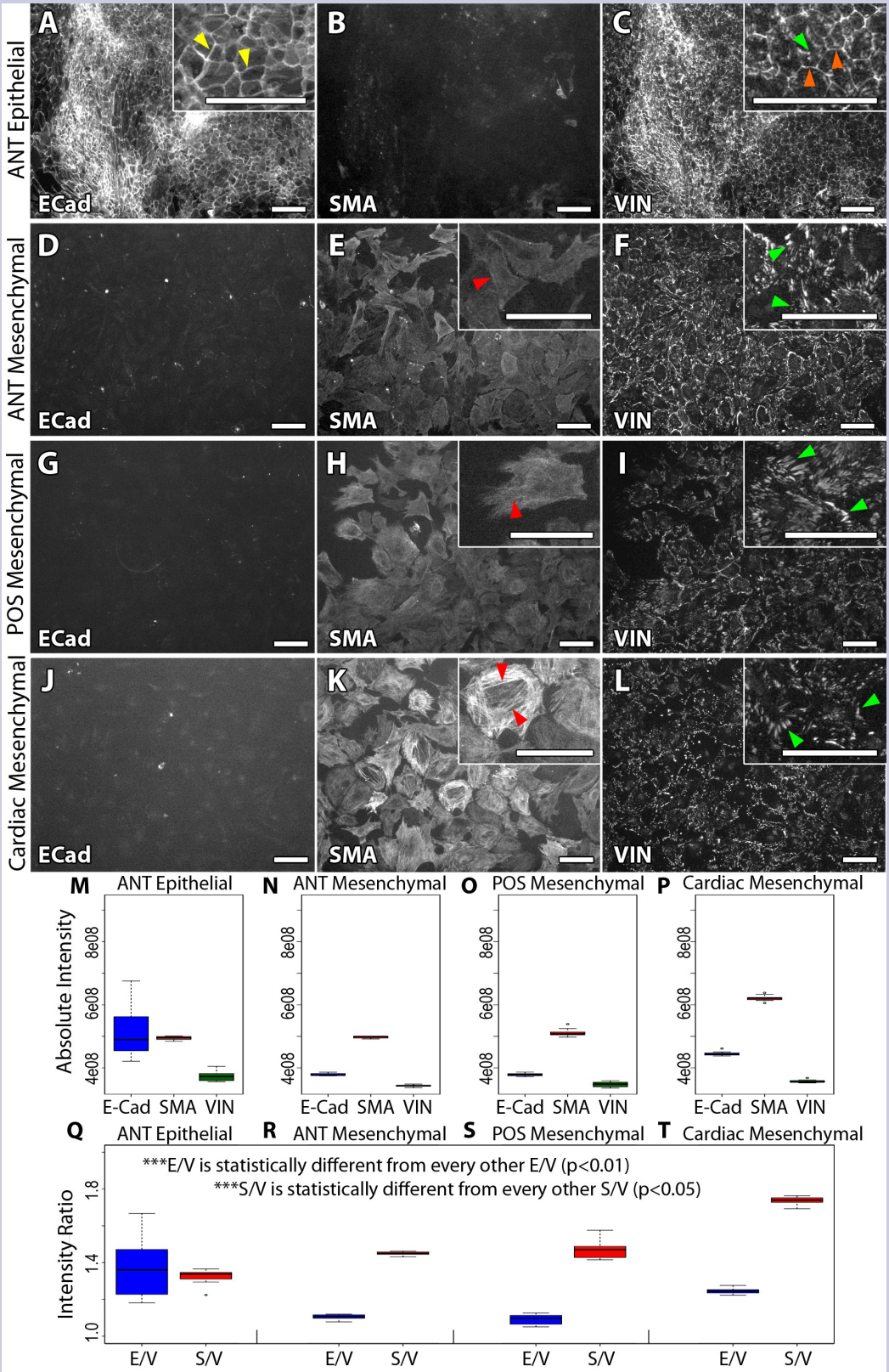

Figure 2: Anterior and posterior primitive streak explants and cardiac cells on glass

Rows represent the same field of a sample image from each of 4 experimental groups: epithelial cells from the anterior primitive streak (A,B,C), mesenchymal cells from the anterior primitive streak (D,E,F), mesenchymal cells from the posterior primitive streak (G,H,I), and mesenchymal cardiac cells (J,K,L). Columns represent each marker: E-Cadherin (A,D,G,J), SMA (B,E,H,K), and Vinculin (C,F,I,L). ALL SCALE BARS ARE 100 µm. (M-T) ECad, SMA, and VIN intensity in anterior and posterior primitive streak explants and cardiac cells on glass. The boxes represent the 25th to 75th percentiles, and the heavy line represents the median. Whiskers represent the top and bottom quartiles of the data. Outliers (less than or greater than 1.5 times the inner quartile range) are denoted by open circles. The absolute intensity value of each marker is displayed for anterior PS explants epithelial cells (M), anterior PS explant mesenchymal cells (N), posterior PS explant mesenchymal cells (O), and mesenchymal cardiac cells (P). ECad and SMA levels are normalized to the VIN staining for each cell type directly beneath (Q,R,S,T).

SMA, ECad, and VIN image quantification distinguishes between cell types

After a cardiac marker screening for smooth muscle α-actin, sarcomeric α-actinin, E-cadherin, N-cadherin, vinculin, β1 integrin, and Nkx2.5, we found that the strongest markers for the PS explants were smooth muscle α-actin (SMA), E-cadherin (ECad), and vinculin (VIN). The heterogeneity of marker expression and morphology in the PS explants prompted us to devise an unbiased imaging method to quantify differences.

Epithelial and mesenchymal regions were exhibited in anterior PS explants. Posterior PS explants and embryonic cardiac cells exhibited only mesenchymal cells. (Regions were classified morphologically. Compact colonies of cells sharing borders were characterized as epithelial. Spread individual cells were characterized as mesenchymal.) The same field was imaged for each of the three markers (SMA, ECad, VIN).

The epithelial region of anterior PS explants on FN-coated glass (Figure 2A,B,C, first row) exhibited ECad staining at the cell-cell borders (Figure 2A inset, yellow arrowheads). Cells appear to form a single layer of cuboidal epithelial cells. There were low levels of SMA staining (Figure 2B) with only 2 or 3 cells in the field expressing SMA. This was not surprising considering that precardiac cells do not re-epithelialize until stage HH6 when they form the splanchnic (ventral) and somatic (dorsal) mesoderm, and SMA translation does not occur until stage HH9 [39]. VIN appears at the cell-cell junctions and is colocalized with ECad at the cell borders (Figure 2C inset, orange arrowheads). In addition, VIN is localized to focal adhesions [52,54] beneath the epithelial cells (Figure 2C inset, green arrowheads).

In the mesenchymal region of anterior PS explants on FN-coated glass (Figure 2, second row), there was little to no ECad staining, which is not surprising given the mesenchymal phenotype. ECad was not localized to the cell borders. The mesenchymal region of the anterior PS exhibited SMA staining, which was interesting since this is the specific region where precardiac cells reside, and SMA is the first cardiac marker. While SMA appears to be ubiquitous throughout the cells, it is also localized to filaments that span the cell (Figure 2E inset, red arrowhead). VIN was visible in focal adhesions throughout the cell but in particular heavily dotting the cell borders (Figure 2F inset, green arrowheads).

The posterior PS on FN-coated glass (Figure 2, third row) exhibited a predominantly mesenchymal phenotype without any epithelial regions. Similar to the mesenchymal region of the anterior PS, there was no ECad staining (Figure 2G). SMA staining was seen throughout the cell and highlighted filaments spanning the cells that generally ran closer to the cell periphery than center (red arrowhead, Figure 2H inset). A difference between the anterior and posterior PS mesenchymal regions was the extent of cell spreading. Across all images, the posterior PS cells (Figure 2, third row) appeared more spread than the mesenchymal anterior region (Figure 2, second row). VIN staining was localized to often elongated focal adhesions (Figure 2I inset, green arrowheads) at the cell periphery and more compact focal adhesions throughout the rest of the cell area.

Cardiac cells explanted from 3-day-old quail embryo hearts were used as a positive control for cardiac differentiation. Cardiac cells on glass (Figure 2, fourth row) were largely negative for ECad, and any visible fluorescence was not localized to the cell border. SMA staining showed very distinct and concentrated actin filaments (Figure 2K inset, red arrowheads) and the highest intensity of the four cell types. Cell spreading was comparable or larger than mesenchymal posterior PS cells. VIN was localized to focal adhesions throughout the cells and concentrated at the cell borders (Figure 2L inset, green arrowheads).

On glass, quantified ECad levels were highest in the epithelial anterior PS explants (Figure 2M), lowest in the mesenchymal regions of the anterior and poster PS explants (Figure 2N,O), and only slightly higher in the cardiac cells (Figure 2P). Posterior PS absolute SMA levels (Figure 2O) were slightly higher than the anterior PS explants (Figure 2M,N), and the cardiac cells had the highest level of SMA staining (Figure 2P). The VIN staining levels were identical for all mesenchymal regions (Figure 2N-P), but were slightly elevated for the anterior epithelial group (Figure 2M).

The ECad and SMA intensities were normalized to VIN intensity. Not surprisingly, E/V is highest in the anterior epithelial region (Figure 2Q), lower in the mesenchymal region of the anterior PS (Figure 2R), and lowest in the posterior PS (Figure 2S). Cardiac cells exhibit a slightly higher E/V still below that of the epithelial anterior PS explants (Figure 2T). E/V comparisons among all groups are different ($p<0.01$). S/V steadily increases across the sample types. The mesenchymal region of the anterior PS has a significantly higher S/V than the epithelial regions ($p<0.01$), and the mesenchymal posterior PS has a higher S/V than the mesenchymal anterior PS ($p<0.05$). As expected, the cardiac cells have the highest S/V ($p<0.001$).

Cardiac marker SMA decreases in presumptive cardiac cells on softer substrate

Explants from the anterior and posterior PS and cardiac cells were cultured on "soft" (250 Pa) and "stiff" (70 kPa) PDMS substrates coated with FN. Overall, the localization of ECad, SMA, and VIN remained similar to our previous experiment on glass; however, the image quantification (Figure 3, Figure 4) showed that precardiac cells in the anterior PS behave differently on "soft" vs. "stiff" PDMS.

On "stiff" FN-coated PDMS (70 kPa), in the epithelial region of anterior PS explants (Figure 3, first row) ECad and VIN were co-localized in the cell-cell borders (Figure 3A inset, yellow arrows and Figure 3C inset, orange arrows). VIN was also localized to focal adhesions throughout the cells (Figure 3C inset, green arrows). As expected, there were low levels of SMA staining in the epithelial anterior PS explants with no distinct localization (Figure 3B).

The mesenchymal region of the anterior PS – the cells fated to form the heart – (Figure 3, second row) showed low levels of

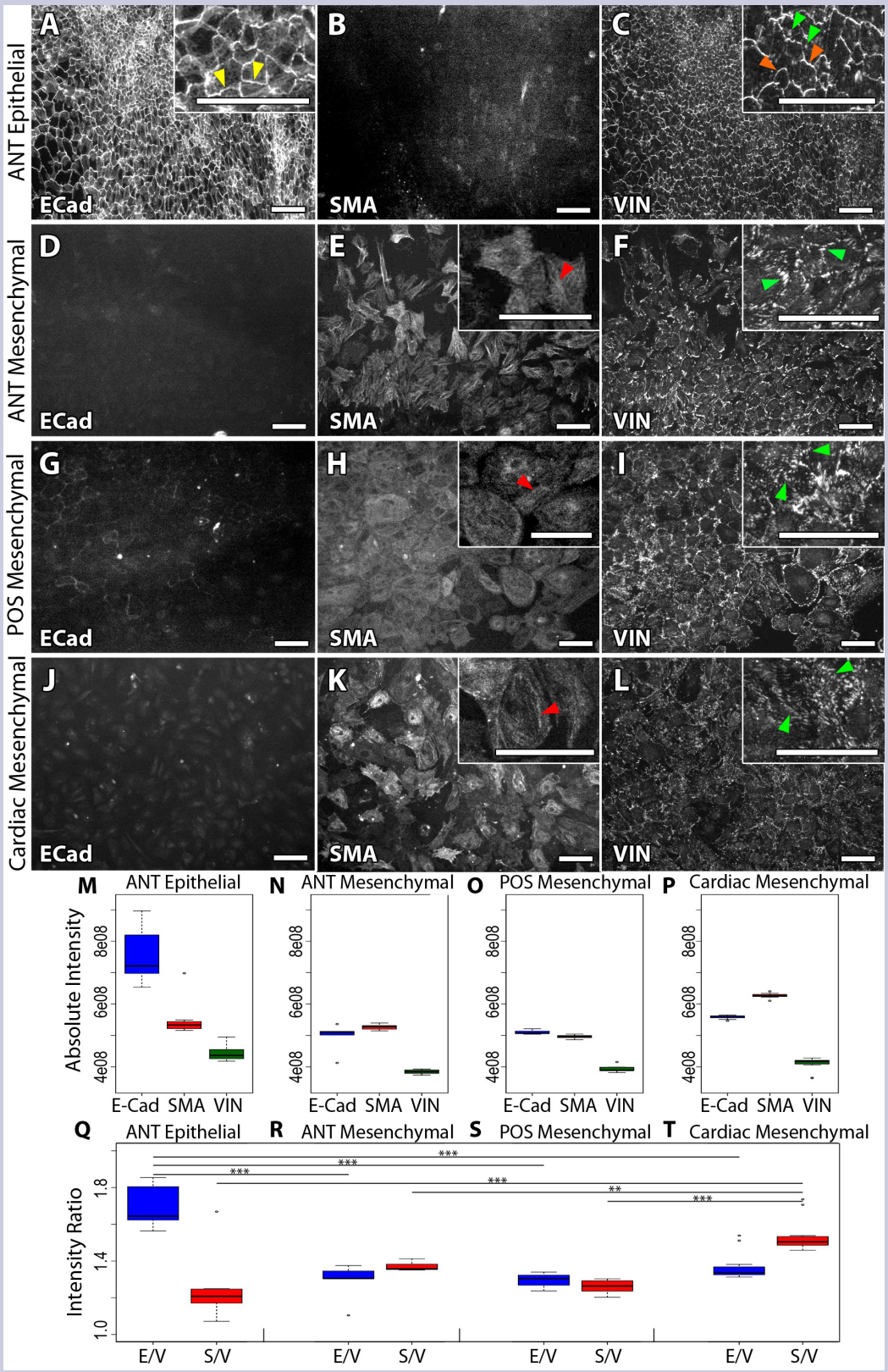

Figure 3: Anterior and posterior primitive streak explants and cardiac cells on "stiff" (70 kPa) PDMS

Rows represent the same field of a sample image from each of 4 experimental groups: epithelial cells from the anterior primitive streak (A,B,C), mesenchymal cells from the anterior primitive streak (D,E,F), mesenchymal cells from the posterior primitive streak (G,H,I), and mesenchymal cardiac cells (J,K,L). Columns represent each marker: E-Cadherin (A,D,G,J), SMA (B,E,H,K), and Vinculin (C,F,I,L). ALL SCALE BARS ARE 100 µm. (M-T) ECad, SMA, and VIN intensity in anterior and posterior primitive streak explants and cardiac cells on "stiff" (70 kPa) PDMS. The boxes represent the 25th to 75th percentiles, and the heavy line represents the median. Whiskers represent the top and bottom quartiles of the data. Outliers (less than or greater than 1.5 times the inner quartile range) are denoted by open circles. The absolute intensity value of each marker is displayed for anterior PS explants epithelial cells (M), anterior PS explant mesenchymal cells (N), posterior PS explant mesenchymal cells (O), and mesenchymal cardiac cells (P). ECad and SMA levels are normalized to the VIN staining for each cell type directly beneath (Q,R,S,T). *** denotes $p<0.001$, ** denotes $p<0.01$, * denotes $p<0.05$

ECad staining (Figure 3D). SMA was present in all cells (Figure 3E) and localized to filaments across the cells (Figure 3E inset, red arrowheads). Faint nuclei are visible as darkened regions in the SMA staining. The anterior PS explants on "stiff" PDMS exhibited VIN localization to focal adhesions throughout the cells (Figure 3F) and preferentially around the cell periphery (Figure 3F inset, green arrowheads).

In the mesenchymal posterior PS region (Figure 3, third row), an interesting pattern was seen in some (approximately 33%) regions of ECad staining. Faint ECad staining was visible in the cell-cell borders (Figure 3G), indicating cell-cell junctions in SMA-expressing cells (Figure 3H). As with cultures on glass, the SMA-expressing cells in posterior PS explants were generally more spread than the anterior PS cells and showed fibers spanning the cells (red arrowhead, Figure 3H inset). VIN was localized to focal adhesions throughout the cell (Figure 3I), particularly those at the cell edge (green arrowheads, Figure 3I inset).

Cardiac cells on "stiff" PDMS (Figure 3, fourth row) showed low ECad levels (Figure 3J). SMA levels appeared to be highest in cardiac cells of the four sample groups (Figure 3K). As previously, SMA was localized to distinct fibers across the cells (Figure 3K inset, red arrowhead) and absent from the nuclear region. Also similarly to cultures on glass, cardiac cells expressed VIN in focal adhesions throughout the cell (Figure 3L) and elongated focal adhesions at the cell borders (Figure 3L inset, green arrowheads).

Figure 3M-T shows all quantified staining for cultures on "stiff" PDMS, which reflect the staining patterns seen in Figure 3A-L. As expected, the E/V of the epithelial anterior PS cells (Figure 3Q) was significantly higher ($p<0.001$) than all other sample groups. Cardiac cell S/V (Figure 3T) was significantly higher than every other sample type ($p<0.001$ compared to anterior epithelial and posterior mesenchymal, $p<0.01$ compared to anterior mesenchymal).

The cultures on "soft" FN-coated PDMS (Figure 4) show similar staining localization patterns to those of "stiff" PDMS, which highlights the necessity of our quantification method for meaningful comparisons between the two that elucidate the connection between cardiac differentiation and substrate stiffness. In the epithelial anterior PS explants (Figure 4, first row), ECad and VIN were co-localized to cell-cell junctions (Figure 4A inset, yellow arrowheads and Figure 4C inset, orange arrowheads, respectively), and there were low levels of SMA staining with no discernible features (Figure 4B).

Mesenchymal regions of the anterior PS (Figure 4, second row), were negative for ECad staining (Figure 4D). SMA expression was localized to filaments across the cells (Figure 4E inset, red arrowhead), and VIN staining was localized to focal adhesions, with a particular presence at the cell edges (Figure 4F inset, green arrowheads).

The mesenchymal posterior PS on FN-coated "soft" PDMS (Figure 4, third row) showed traces of ECad at the cell-cell boundaries of SMA-expressing cells, similar to the same cultures on "stiff" PDMS (Figure 4G). SMA-expressing cells (Figure 4H) were generally more spread than that anterior mesenchymal cells, and SMA was localized to actin filaments (Figure 4H inset, red arrowheads) often traversing the non-central periphery of the cells. VIN staining was seen in focal adhesions concentrated at the cell edges (Figure 4I inset, green arrowheads).

Cardiac cells (Figure 4, fourth row) exhibited low levels of ECad staining (Figure 4J) but the highest levels of SMA staining across the sample groups on "soft" PDMS. SMA was localized to filaments throughout the cell (Figure 4K inset, red arrowheads). VIN was visible in elongated focal adhesions at the cell edges (Figure 4L inset, green arrowheads).

On "soft" PDMS (Figure 4Q-T), E/V was again highest in the epithelial anterior PS explants (Figure 4Q) ($p<0.05$ compared to the mesenchymal region of the anterior PS, $p<0.01$ compared to the posterior PS, $p<0.001$ compared to cardiac cells). Cardiac cells showed the highest S/V (Figure 4T) ($p<0.001$ compared to other sample types). S/V for anterior and posterior PS mesenchymal regions was significantly higher than anterior PS epithelial regions ($p<0.05$ and $p<0.01$, respectively).

Figure 5 shows side-by-side comparisons of the same sample type on different substrates stiffnesses. First, in the epithelial region of the anterior PS cultures, there is no difference in the E/V and S/V values between "stiff" (Figure 5A) and "soft" (Figure 5B) PDMS. We can conclude that the substrate stiffness did not affect the epithelial region of the anterior PS explants.

Next, in the mesenchymal region of the anterior PS, which is the cell type of greatest interest in this study due to its in vivo cardiac fate, the S/V ratio is significantly higher on "stiff" PDMS ($p<0.001$) compared to "soft" PDMS (Figure 5C,D). We conclude that mesenchymal cells from the anterior PS are influenced by substrate stiffness in terms of SMA expression.

Side-by-side comparison of the posterior PS explants on "soft" and "stiff" PDMS (Figure 5E,F) revealed a significant ($p<0.001$) increase in E/V on "soft" PDMS. This result suggests that the faint ECad staining present at cell-cell borders in this sample group increased on the softer substrate. We can conclude that substrate stiffness affects cells from the posterior PS in terms of ECad expression.

In the cardiac cell cultures on FN-coated "soft" and "stiff" PDMS, there were no statistical differences between E/V and S/V (Figure 5G,H). This finding is significant because both the anterior and posterior PS mesenchymal cells showed differences on "soft" and "stiff" PDMS, which suggests that cardiomyocytes from a 3-day-old quail embryo may have matured past this point of sensitivity to substrate stiffness as indicated by SMA and ECad expression.

In summary, the most significant results in this study are as follows: 1) Anterior mesenchymal PS explants (cardiac-fated cells) showed decreased S/V on "soft" compared to "stiff" PDMS. 2) Posterior mesenchymal PS explants showed increased E/V on "soft" compared to "stiff" PDMS. 3) Cardiac cells did not show different E/V or S/V on "soft" or "stiff" PDMS. 4) Cardiac cells had

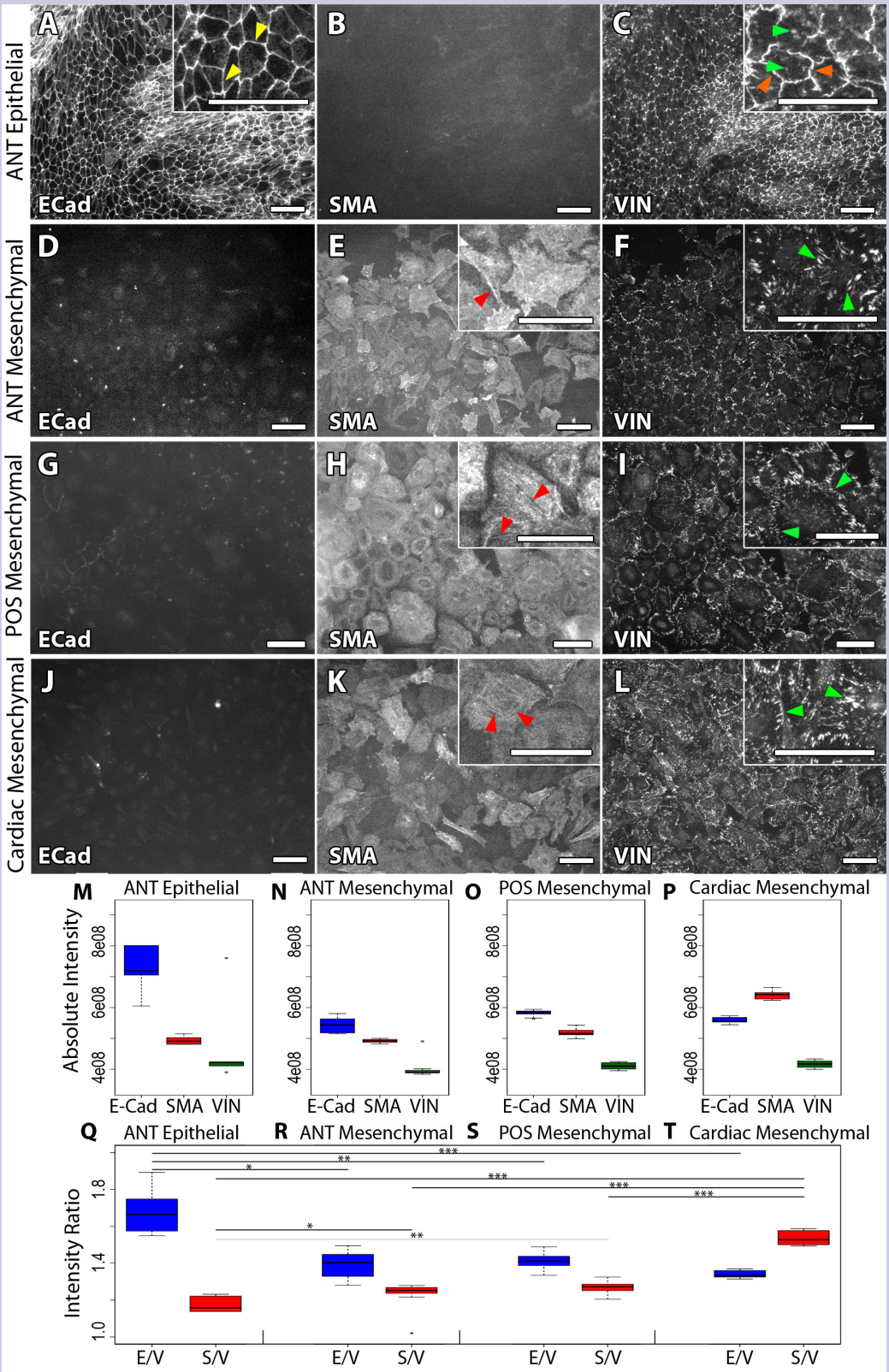

Figure 4: Anterior and posterior primitive streak explants and cardiac cells on "soft" (250 Pa) PDMS

Rows represent the same field of a sample image from each of 4 experimental groups: epithelial cells from the anterior primitive streak (A,B,C), mesenchymal cells from the anterior primitive streak (D,E,F), mesenchymal cells from the posterior primitive streak (G,H,I), and mesenchymal cardiac cells (J,K,L). Columns represent each marker: E-Cadherin (A,D,G,J), SMA (B,E,H,K), and Vinculin (C,F,I,L). ALL SCALE BARS ARE 100 µm. (M-T) ECad, SMA, and VIN intensity in anterior and posterior primitive streak explants and cardiac cells on "soft" (250 Pa) PDMS. The boxes represent the 25th to 75th percentiles, and the heavy line represents the median. Whiskers represent the top and bottom quartiles of the data. Outliers (less than or greater than 1.5 times the inner quartile range) are denoted by open circles. The absolute intensity value of each marker is displayed for anterior PS explants epithelial cells (M), anterior PS explant mesenchymal cells (N), posterior PS explant mesenchymal cells (O), and mesenchymal cardiac cells (P). ECad and SMA levels are normalized to the VIN staining for each cell type directly beneath (Q,R,S,T). *** denotes $p<0.001$, ** denotes $p<0.01$, * denotes $p<0.05$

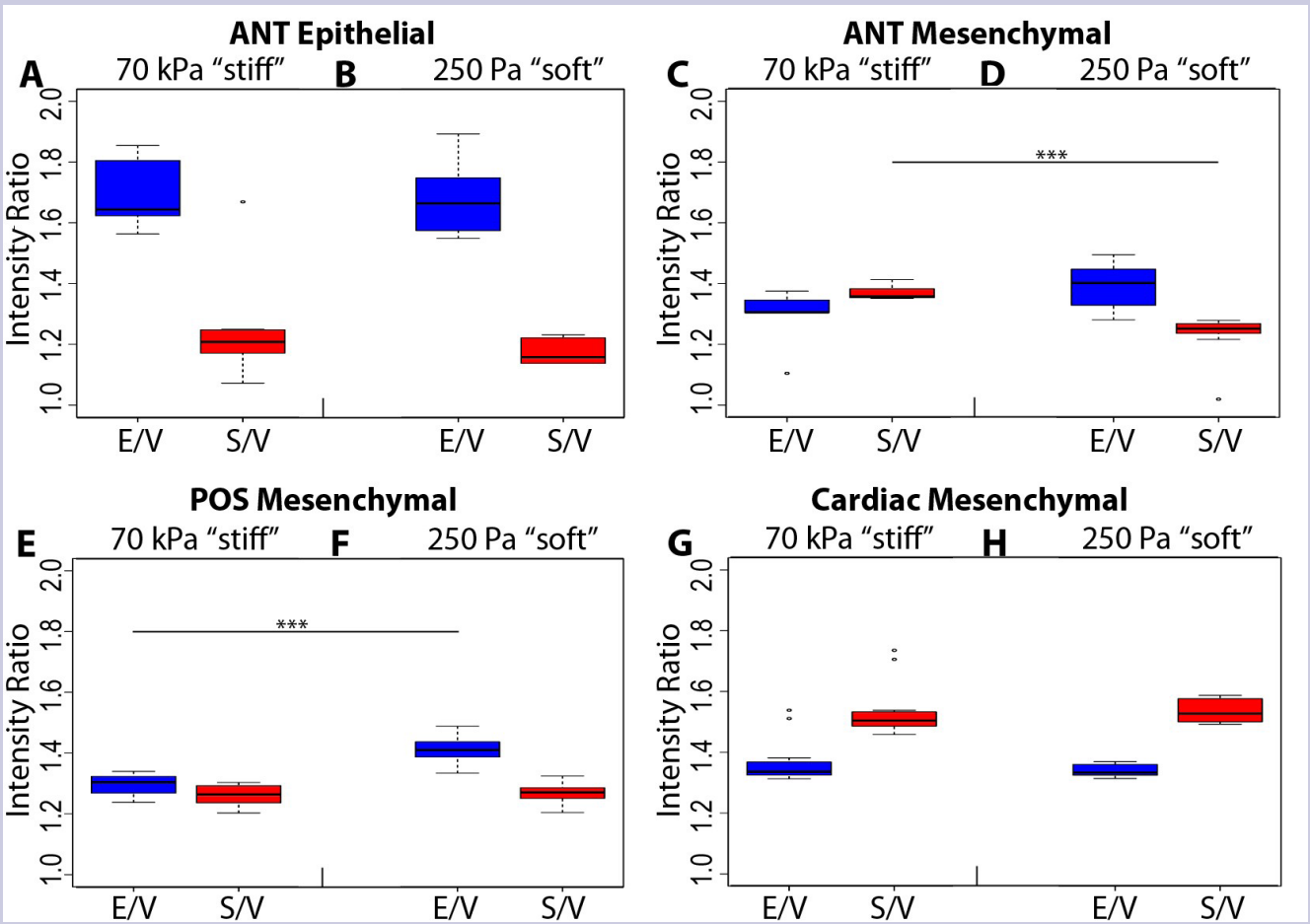

Figure 5: Side-by-side comparison of ECad/VIN and SMA/VIN intensity ratios on "stiff" (70 kPa) and "soft" (250 Pa) PDMS
(A,B) Epithelial region of anterior primitive streak explants on A) "stiff" (70 kPa) and B) "soft" (250 Pa) PDMS. (C,D) Mesenchymal region of anterior primitive streak explants on C) "stiff" (70 kPa) and D) "soft" (250 Pa) PDMS. (E,F) Mesenchymal posterior primitive streak explants on E) "stiff" (70 kPa) and F) "soft" (250 Pa) PDMS. (G,H) mesenchymal cardiac cells on G) "stiff" (70 kPa) and H) "soft" (250 Pa) PDMS. *** denotes $p<0.001$

a higher S/V than all cell types on "soft" and "stiff" substrates.

Sarcomeric myosin heavy chain expression is not altered by changes in substrate stiffness in primitive streak cells

Because we detected significant differences in SMA staining in cardiac-fated cells on "soft" and "stiff" substrates, we next stained for sarcomeric myosin heavy chain as a means to detect a functional difference between the cultures. Samples were stained with MF20 and sytox, and images were imported into Matlab to calculate the percent of cells expressing sarcomeric myosin heavy chain. In the anterior (Figure 6A,B,G,H, first row) and posterior (Figure 6C,D,I,J, second row) PS cultures, myosin appeared to be granulated (Figure 6C,G,I insets) throughout the cell, similar to the cardiac cultures (Figure 6E,K insets). In the anterior PS cultures on "stiff" PDMS (Figure 6A,B), there were low levels of MF20 staining, which appeared to be elevated on "soft" PDMS (Figure 6G,H). However, image analysis and a 2-way ANOVA indicated no statistical differences between the percent of cells positive for MF20 between the two groups (Figure 6M,N), which indicates that a more sensitive test may be required to quantify the observations. The posterior PS explants (Figure 6, second row) similarly did not show significant differences (Figure 6M,N). The cardiac cell cultures (Figure 6, third row) exhibited a higher percentage of MF20-expressing cells on the "soft" PDMS compared to "stiff" PDMS (Figure 6E,F,K,L,M,N). Interestingly, while cardiac cells do not express different levels of SMA on different substrate stiffnesses, they exhibit higher levels of sarcomeric myosin heavy chain on "soft" PDMS, suggesting that the response to substrate stiffness changes over time with different cardiac cell markers.

Changes in substrate stiffness do not alter the prevalence of beating cultures

We observed the prevalence of beating cells across all sample types to detect a functional difference in the cardiac-fated cells' response to substrate stiffness. A chi-squared test determined that there were no differences between the number of beating cultures on any substrate and cell type (Table 2), which shows a further need for stage-by-stage analysis of cardiogenesis, because differentiated cardiac cells from formed embryonic hearts show substrate stiffness preferences [20].

DISCUSSION

Our results show for the first time that cardiac-fated cells are susceptible to cardiac-marker expression changes based on substrate stiffness. Cardiac-fated cells from the PS express

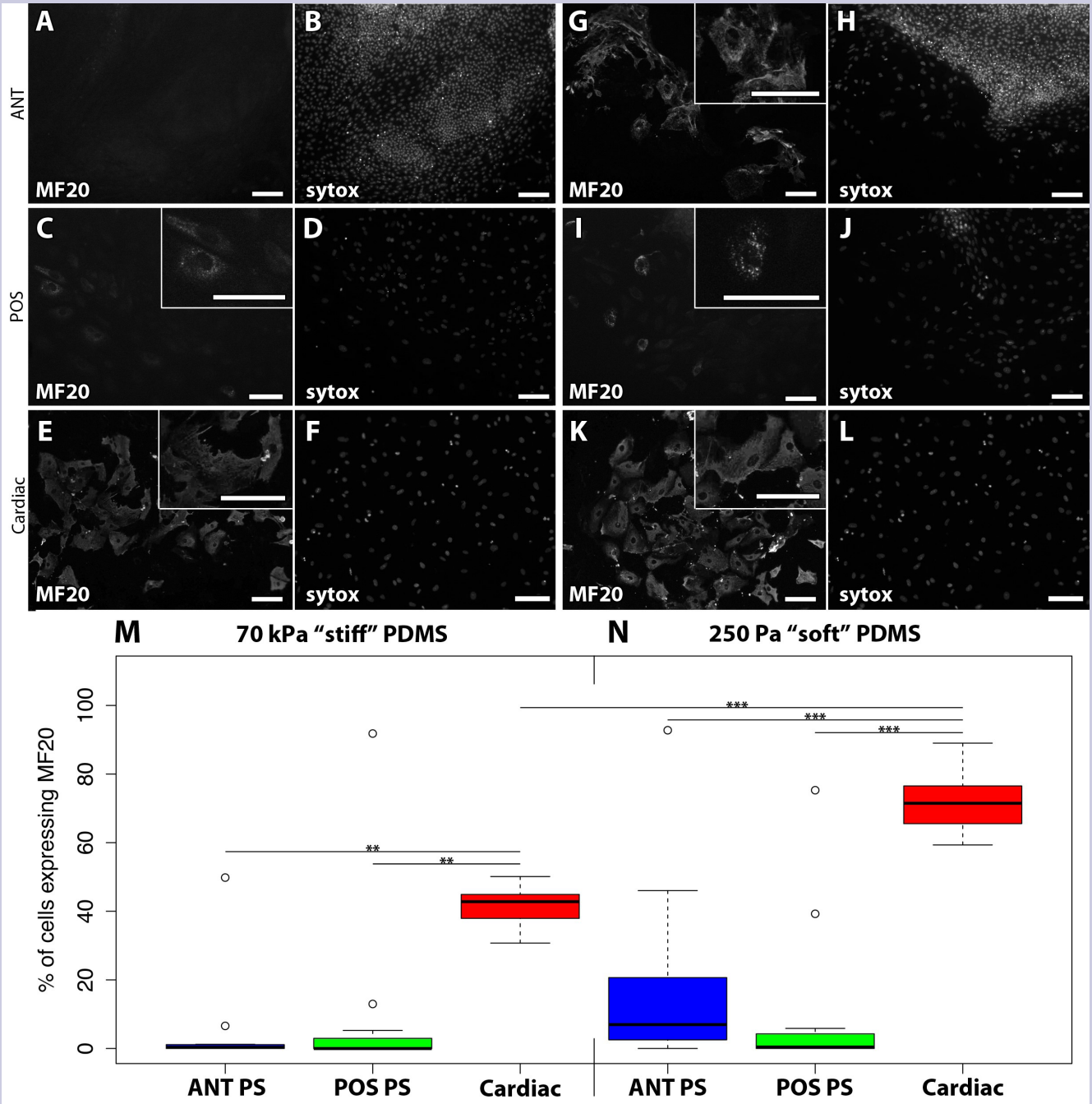

Figure 6: Sarcomeric myosin heavy chain and nuclei immunofluorescence staining of anterior and posterior primitive streak explants and cardiac cells on "stiff" (70 kPa) (A-F) and "soft" (250 Pa) (G-L) PDMS

Rows represent the same field of a sample image from each of 3 experimental groups: anterior primitive streak (A,B,G,H), posterior primitive streak (C,D,I,J), and cardiac cells (E,F,K,L). Columns represent each marker: MF20 (sarcomeric myosin heavy chain) (A,C,E,G,I) and sytox (nuclei) (B,D,F,H,J). The first 2 columns represent samples on "stiff" (70 kPa) PDMS (A-F) and the second 2 columns (G-L) represent samples on "soft" (250 Pa) PDMS. ALL SCALE BARS ARE 100 µm. (M,N) MF20 immunofluorescence staining as a percent of total cell (nuclei) count in anterior and posterior primitive streak explants and cardiac cells on (M) "stiff" (70 kPa) and (N) "soft" (250 Pa) (250 Pa) PDMS. The boxes represent the 25th to 75th percentiles, and the heavy line represents the median. Whiskers represent the top and bottom quartiles of the data. Outliers (less than or greater than 1.5 times the inner quartile range) are denoted by open circles. On (M) "stiff" (70 kPa) and (N) "soft" (250 Pa) (250 Pa) PDMS, cardiac cells expressed MF20 in a higher percentage of cells than the primitive streak explants. ANT PS = anterior primitive streak, POS PS = posterior primitive streak. ** denotes $p<0.01$, *** denotes $p<0.001$

Table 2: Beating cultures per sample count

Cell type	70 kPa PDMS	250 Pa PDMS
Anterior primitive streak	1/35	4/35
Posterior primitive streak	5/35	1/35
Cardiac cells	36/36	36/36
Abbreviations: polydimethylsiloxane (PDMS)		

statistically higher levels of SMA, the first cardiac marker, on "stiff" compared to "soft" PDMS, which is suggestive of a transition toward cardiac differentiation. In addition, higher levels of SMA indicate mesenchymal-like behavior on "stiff" PDMS. (Posterior PS cells similarly expressed higher levels of ECad on "soft" compared to "stiff" PDMS, suggesting epithelial-like behavior on "soft" PDMS and mesenchymal-like behavior on "stiff" PDMS.) An important implication of these findings is that the formulation

of hiPSC and other cell-differentiation protocols would do well to include the characterization of desired substrate stiffness over time to determine and optimize the conditions to produce a targeted cell type. Further, the study indicates the importance of characterizing cells' response to the moduli of scaffolds in cardiac tissue engineering applications. Future developmental cardiac studies would also benefit from taking into account the mechanical microenvironment during cardiogenesis. It was interesting to note that the cardiac cells from 3-day-old embryonic hearts did not exhibit the same substrate-dependent SMA expression as earlier (HH3) cardiac-fated cells, because later-stage embryonic cardiomyocytes have demonstrated substrate-stiffness sensitivity [7,20,21]. This finding suggests that cardiac cells' responsiveness to substrate and tissue stiffness may be in flux over time. Taken together, these results emphasize the relevance of examining the rapidly-changing biochemical and biophysical environments and the cells' sensitivity to both at each distinct stage of development. The results also indicate a potential benefit for taking into account the effect of the mechanical microenvironment at each phase of cell-differentiation protocols in order to improve differentiation success rates for targeted cell phenotypes.

When examining the expression of sarcomeric myosin heavy to chain as a means to determine if the differences in SMA and ECad staining have functional consequences to the embryo, we found only that the percentage of cells expressing sarcomeric myosin heavy chain increased in the differentiated cardiac cells, not in the PS cardiac-fated cells. The cardiac cells expressed higher levels of sarcomeric myosin heavy chain on "soft" compared to "stiff" PDMS, and the cardiac cells on both substrates expressed significantly higher sarcomeric myosin heavy chain than the anterior and posterior PS cells on each substrate. These results elucidate the continuous and dynamic sensitivity to (and effects of) changing substrate stiffnesses within the embryo during heart development, which confirm the importance of future characterization of substrate stiffness in cell differentiation, developmental, and tissue engineering applications.

A limitation of this study is that small cell counts from the embryo did not allow for reliable flow cytometry. Because we were able to determine differences in SMA and ECad staining in PS cells, further insights may be obtained via sub-cellular characterization, ideally, a method akin to "localized flow cytometry" that would have the benefit of the sensitivity of flow cytometry, but would not require the cells to be trypsinized and lose their spatial significance within the cultures. We would like to move to a finer "map" of staining using smaller windows within the 10x fields to display more localized immunofluorescence staining. In addition, further development and characterization of a finer range of substrate stiffnesses scaling up from the physiologic "soft" (250 Pa) substrate created for this study would enable a more nuanced exploration of the effect of changes to substrate stiffness on cardiac marker expression. Finally, we would be interested in expanding stages of cardiac-fated cell explants (HH5, HH7) and using additional downstream cardiac markers such as sarcomeric myosin to examine sensitivity to substrate stiffness over a broader range of differentiation stages in the embryo.

One of the related themes to this work in addition to cardiac differentiation is EMT because of EMT's shown dependence on substrate stiffness [55]. SMA is the first cardiac marker, but it has also been used as a marker of EMT [56]. Because EMT has been shown to be effected by substrate stiffness, the differentiation of cells in the streak undergoing EMT during gastrulation [57] may also be dependent on substrate stiffness. We acknowledge that there may be redundant mechanisms for upregulating SMA in precardiac cells, because these cells undergo EMT just 1 stage before transcribing SMA. In future studies, flow cytometry and in situ hybridization may be a good next step to more fully characterize the transcription and translation of more cardiac markers in these PS explants.

One advantage of this study is that we are studying the effect of substrate stiffness on cardiogenesis with isolated precardiac cells as opposed to an undifferentiated stem cell line. All necessary developmental cues up to the point of localization to the anterior PS have taken place, and we explant the precardiac cells 2 stages prior to the transcription of the first heart marker, SMA. Nonetheless, we hope that the results of this study will be advantageous for ongoing studies of developing cardiac cell therapies from induced pluripotent stem cells (iPSCs) [58] and mesenchymal stem cells [59,60].

CONCLUSION

Here we have shown that substrate stiffness affects the behavior of anterior and posterior PS cells, the former of which are fated to form the heart during embryogenesis. We hope that the results of this study will not only encourage further exploration of the effects of substrate stiffness on development and stem cell differentiation for therapeutic applications, but that studies of the effects of substrate stiffness will account for the importance of mechanical characterization so that results can be understood in the context of the true mechanical environment, specifically, substrate stiffness in vivo.

ACKNOWLEDGMENT

The authors would like to thank Dr. Wenwei Xu for providing beaded AFM cantilevers and Dr. Julia Raykin for Matlab consulting. This work was supported by the National Science Foundation (Grant #1000604 and CMMI 1538161 to TS). JH was partially supported by the NIH Biotechnology Training Program on Cell and Tissue Engineering (NIH T32 GM008433).

DISCLOSURE

The authors declare no conflicts of interest.

REFERENCES

1. Seong J, Wang N, Wang Y. Mechanotransduction at focal adhesions: from physiology to cancer development. J Cell Mol Med. 2013.

2. Discher, D E et. al. Tissue cells feel and respond to the stiffness of their substrate. Science. 2005; 310: 1139.

3. Vogel V, Sheetz M. Local force and geometry sensing regulate cell

functions. Nat Rev Mol Cell Biol. 2006 ; 7: 265 – 275.

4. Balgude A, Yu X, Szymanski A, Bellamkonda R. Agarose gel stiffness determines rate of DRG neurite extension in 3d cultures. Biomaterials. 2001; 22(10): 1077–1084.

5. Pelham R, Wang Y. Cell locomotion and focal adhesions are regulated by the mechanical properties of the substrate. Biol Bull. 1998; 194: 348-350.

6. Yeh Y, Hur S, Chang J, Wang K, Chiu J, Li Y, Chien S. Matrix stiffness regulates endothelial cell proliferation through septin 9. PLoS One. 2012; 7(10): 46889.

7. Forte G, et. al, Substrate stiffness modulates gene expression and phenotype in neonatal cardiomyocytes in vitro. Tissue Eng Part A. 2012: 18(17-18): 1837-1848.

8. Geiger B, Spatz J, Bershadsky, A. Environmental sensing through focal adhesions. Nat Rev Mol Cell Biol. 2009; 10(1): 21-33.

9. Kong H, Polte T, Alsberg E, Mooney D. Fret measurements of cell-traction forces and nano-scale clustering of adhesion ligands varied by substrate stiffness. Proc Natl Acad Sci. 2005; 102: 4300-4305.

10. Ng M, Besser A, Danuser G, Brugge J. Substrate stiffness regulates cadherin-dependent collective migration through myosin-ii contractility. J Cell Biol. 2012; 199(3): 545-563.

11. Lo C, Wang H, Dembo M, Wang Y. Cell movement is guided by the rigidity of the substrate. Biophys J. 2000; 79: 144-152.

12. Peyton S, Putnam A. Extracellular matrix rigidity governs smooth muscle cell motility in a biphasic fashion. J Cell Physiol. 2005; 204: 198-209.

13. Li X et. al. Effect of substrate stiffness on the functions of rat bone marrow and adipose tissue derived mesenchymal stem cells in vitro. J Biomed Mater Res A. 2013; 102(4): 1092-1101.

14. Engler A, Sen S, Sweeney H, Discher D. Matrix elasticity directs stem cell lineage specification. Cell. 2006; 126(4): 677-689.

15. Levental K, Yu H, Kass L, Lakins J, Egeblad M, Erler J, Fong S, Csiszar K, Giaccia A, Weninger W, Yamauchi M, Gasser D, Weaver V. Matrix crosslinking forces tumor progression by enhancing integrin signaling. Cell. 2009; 139(5): 891-906.

16. Nelson C, Bissell M. Of extracellular matrix, scaffolds, and signaling: tissue architecture regulates development, homeostasis, and cancer. Annu Rev Cell Dev Biol. 2006; 22: 287-309.

17. Keller R, Davidson LA, Shook DR. How we are shaped: The biomechanics of gastrulation. Differentiation. 2003; 71: 171-205.

18. Burridge P, Matsa E, Shukla P, Lin Z, Churko J, Ebert A, Lan F, Diecke S, Huber B, Mordwinkin N, Plews J, Abilez O, Cui B, Gold J, Wu J. Chemically defined generation of human cardiomyocytes. Nature Methods. 2014; 11(8): 855-860.

19. Berry, Mark F, Engler, Adam J, Woo Y Joseph, Pirolli, Timothy J, Bish, Lawrence T, Jayasankar, Vasant, Morine, Kevin J, Gardner, Timothy J, Discher, Dennis E, Sweeney, H Lee. Mesenchymal stem cell injection after myocardial infarction improves myocardial compliance. American Journal of Physiology - Heart and Circulatory Physiology. 2006; 290(6): H2196-H2203.

20. Engler AJ, Carag-Krieger C, Johnson CP, Raab M, Tang HY, Speicher DW, Sanger JW, Sanger JM, Discher DE. Embryonic cardiomyocytes beat best on a matrix with heart-like elasticity: scar-like rigidity inhibits beating. Journal of Cell Science. 2008; 121(22): 3794-3802.

21. Young J, Engler A. Hydrogels with time-de pendent material properties enhance cardiomyocyte differentiation in vitro. Biomaterials. 2011; 32(4): 1002-1009.

22. Hamburger V, Hamilton HL. A series of normal stages in the development of the chick embryo. J Morphol. 1951; 88(1): 49-92.

23. Zamir EA, Srinivasan V, Perucchio R, Taber LA. Mechanical asymmetry in the embryonic chick heart during looping. Annals of biomedical engineering. 2003; 31(11): 1327-1336.

24. Zamir EA, Taber LA. Material properties and residual stress in the stage 12 chick heart during cardiac looping. Journal of biomechanical engineering. 2004: 126(6); 823-830.

25. Eyal-Giladi H, Kochav S. From cleavage to primitive streak formation: a complementary normal table and a new look at the first stages of the development of the chick. I. General morphology. Developmental biology. 1976; 49(2): 321-337.

26. Hatada Y, Stern CD. A fate map of the epiblast of the early chick embryo. Development. 1994; 120(10): 2879-2889.

27. Garcia-Martinez, Schoenwolf GC. Primitive-streak origin of the cardiovascular system in avian embryos. Dev Biol. 1993; 159(2): 706-719.

28. Schultheiss TM, Xydas S, Lassar AB. Induction of avian cardiac myogenesis by anterior endoderm. Development. 1995; 121(12): 4203-4214.

29. Matsui H, Sakabe M, Sakata H, Yanagawa N, Ikeda K, Yamagishi T, Nakajima Y. Induction of initial heart alpha-actin, smooth muscle alpha-actin, in chick pregastrula epiblast: the role of hypoblast and fibroblast growth factor-8. Development, Growth, and Differentiation. 2008; 50(3): 143-157.

30. Colas JF, Lawson A, Schoenwolf GC. Evidence that translation of smooth muscle alpha-actin mRNA is delayed in the chick promyocardium until fusion of the bilateral heart-forming regions. Dev Dyn. 2000; 218(2): 316-330.

31. Rawles ME. The heart-forming areas of the early chick blastoderm. Physiol Zool. 1943; 16: 22-43.

32. Linask KK. N-cadherin localization in early heart development and polar expression of Na+,K(+)-ATPase, and integrin during pericardial coelom formation and epithelialization of the differentiating myocardium. Dev Biol. 1992; 151(1): 213-224.

33. Moreno-Rodriguez RA, Krug EL, Reyes L, Villavicencio L, Mjaatvedt CH, Markwald RR. Bidirectional fusion of the heart-forming fields in the developing chick embryo. Dev Dyn. 2006; 235(1): 191-202.

34. DeRuiter MC, Poelmann RE, Mentink MM, Vaniperen L, Gittenberger-De Groot AC. Early formation of the vascular system in quail embryos. Anat Rec. 1993; 235(2): 261-74.

35. Stalsberg H, DeHaan RL. The precardiac areas and formation of the tubular heart in the chick embryo. Dev Biol. 1969; 19(2): 128-159.

36. Gannon M, Bader D. Initiation of cardiac differentiation occurs in the absence of anterior endoderm. Development. 1995; 121(8): 2439-2450.

37. Han Y, Dennis J, Cohen-Gould L, Bader D, Fischman D. Expression of sarcomeric myosin in the presumptive myocardium of chicken embryos occurs within six hours of myocyte commitment. Dev Dyn.

1992; 193(3): 257-265.

38. Yutzey KE, Rhee JT, Bader D. Expression of the atrial-specific myosin heavy chain AMHC1 and the establishment of anteroposterior polarity in the developing chicken heart. Development, 1994; 120: 871-883.

39. Sugi Y, Lough J. Onset of expression and regional deposition of alpha-smooth and sarcomeric actin during avian heart development. Dev Dyn. 1992; 193(2): 116-124.

40. Eisenberg LM, Eisenberg CA. An in vitro analysis of myocardial potential indicates that phenotypic plasticity is an innate property of early embryonic tissue. Stem Cells and Development. 2004; 13(6): 614-624.

41. Ruzicka DL, Schwartz RJ. Sequential activation of alpha-actin genes during avian cardiogenesis: vascular smooth muscle alpha-actin gene transcripts mark the onset of cardiomyocyte differentiation. Journal of Cell Biology. 1988; 107(6 Pt 2): 2575-2586.

42. Matsui H, Ikeda K, Nakatani K, Sakabe M, Yamagishi T, Nakanishi T, Nakajima Y. Induction of initial cardiomyocyte α-actin smooth muscle α-actinin cultured avian pregastrula epiblast: A role for nodal and bmp antagonist. Dev Dyn. 2005; 233(4): 1419-1429.

43. Ladd AN, Yatskievych TA, Antin PB. Regulation of avian cardiac myogenesis by activin/tgfbeta and bone morphogenetic proteins. Dev Biol. 1998; 204(2): 407-419.

44. Yatskievych TA, Ladd AN, Antin PB. Induction of cardiac myogenesis in avian pregastrula epiblast: the role of the hypoblast and activin. Development. 1997; 124(13): 2561-2570.

45. Sugi Y, Lough J. Activin-a and fgf-2 mimic the inductive effects of anterior endoderm on terminal cardiac myogenesis in vitro. Dev Biol. 1995; 168(2): 567-574.

46. Antin PB, Taylor RG, Yatskievych T. Precardiac mesoderm is specified during gastrulation in quail. Dev Dyn. 1994; 200(2): 144-154.

47. Gonzalez-Sanchez A, Bader D. In vitro analysis of cardiac progenitor cell differentiation. Dev Biol. 1990; 139(1): 197-209.

48. Schultheiss TM, Burch JB, Lassar AB. A role for bone morphogenic proteins in the induction of cardiac myogenesis. Genes & Development. 1997; 8: 451-462.

49. Henkels J, Oh J, Xu W, Owen D, Sulchek T, Zamir E. Spatiotemporal mechanical variation reveals critical role for rho kinase during primitive streak morphogenesis. Ann Biomed Eng. 2013; 41(2): 421-432.

50. Xu W, Chahine N, Sulchek T. Extreme hardening of PDMS thin films due to high compressive strain and confined thickness. Langmuir. The ACS journal of surfaces and colloids. 2011; 27(13): 8470-8477.

51. New, DA T. A new technique for the cultivation of the chick embryo in vitro. J. Embryol. exp. Morph. 1955; 3 part 4; 320-331.

52. Dumbauld D, Michael K, Hanks S, García A. Focal adhesion kinase-dependent regulation of adhesive forces involves vinculin recruitment to focal adhesions. Biol Cell. 2010; 102(4): 203-213.

53. García A, Vega M, Boettiger D. Modulation of cell proliferation and differentiation through substrate-dependent changes in fibronectin conformation. Mol Biol Cell. 1999; 10(3): 785-798.

54. Dumbauld, David W, Lee, Ted T, Singh, Ankur, Scrimgeour, Jan, Gersbach, Charles A, Zamir, Evan A, Fu, Jianping, Chen, Christopher S, Curtis, Jennifer E, Craig, Susan W, García, Andrés J. How vinculin regulates force transmission. PNAS. 1999; 110(24): 9788-9793.

55. Brown A, Fiore V, Sulchek T, Barker T. Physical and chemical microenvironmental cues orthogonally control the degree and duration of fibrosis-associated epithelial to mesenchymal transition. J Pathol. 2012; 229(1): 25-35.

56. Zeisberg M, Neilson E. Biomarkers for epithelial-mesenchymal transitions. J Clin Invest. 2009; 119(6): 429–1437.

57. Nakaya Y, Sheng G. Epithelial to mesenchymal transition during gastrulation-an embryological view. Develop Growth Differ. 2008; 50: 755-766.

58. Kamakura T, Makiyama T, Sasaki K, Yoshida Y, Wuriyanghai Y, Chen J, Hattori T, Ohno S, Kita T, Horie M, Yamanaka S, Kimura T. Ultrastructural maturation of human-induced pluripotent stem cell-derived cardiomyocytes in a long-term culture. Circulation Journal. 2013; 77(5): 1307-1314.

59. Li Z, Guo X, Palmer A, Das H, Guan J. High-efficiency matrix modulus-induced cardiac differentiation of human mesenchymal stem cells inside a thermosensitive hydrogel. Acta Biomater. 2012; 8(10): 3586-3595.

60. Pittenger MF, Martin BJ. Mesenchymal stem cells and their potential as cardiac therapeutics. Circ Res. 2004; 95: 9-20.